



HAL
open science

Multiplexed readout of four qubits in 3D circuit QED architecture using a broadband Josephson parametric amplifier

Suman Kundu, Nicolas Gheeraert, Sumeru Hazra, Tanay Roy, Kishor Salunkhe, Meghan Patankar, R. Vijay

► To cite this version:

Suman Kundu, Nicolas Gheeraert, Sumeru Hazra, Tanay Roy, Kishor Salunkhe, et al.. Multiplexed readout of four qubits in 3D circuit QED architecture using a broadband Josephson parametric amplifier. *Applied Physics Letters*, 2019, 114 (17), pp.172601. 10.1063/1.5089729 . hal-04062425

HAL Id: hal-04062425

<https://hal.science/hal-04062425>

Submitted on 11 May 2023

HAL is a multi-disciplinary open access archive for the deposit and dissemination of scientific research documents, whether they are published or not. The documents may come from teaching and research institutions in France or abroad, or from public or private research centers.

L'archive ouverte pluridisciplinaire **HAL**, est destinée au dépôt et à la diffusion de documents scientifiques de niveau recherche, publiés ou non, émanant des établissements d'enseignement et de recherche français ou étrangers, des laboratoires publics ou privés.

RESEARCH ARTICLE | MAY 01 2019

Multiplexed readout of four qubits in 3D circuit QED architecture using a broadband Josephson parametric amplifier

Suman Kundu; Nicolas Gheeraert; Sumeru Hazra; ... et. al



Appl. Phys. Lett. 114, 172601 (2019)

<https://doi.org/10.1063/1.5089729>



CrossMark

Articles You May Be Interested In

An architecture for integrating planar and 3D cQED devices

Appl. Phys. Lett. (July 2016)

Fast flux control of 3D transmon qubits using a magnetic hose

Appl. Phys. Lett. (January 2021)

Are there Local Minima in the Magnetic Monopole Potential in Compact QED?

AIP Conference Proceedings (April 2005)

Time to get excited.
Lock-in Amplifiers – from DC to 8.5 GHz

[Find out more](#)

Zurich Instruments

Multiplexed readout of four qubits in 3D circuit QED architecture using a broadband Josephson parametric amplifier

Cite as: Appl. Phys. Lett. **114**, 172601 (2019); doi: [10.1063/1.5089729](https://doi.org/10.1063/1.5089729)

Submitted: 22 January 2019 · Accepted: 16 April 2019 ·

Published Online: 1 May 2019




View Online



Export Citation



CrossMark

Suman Kundu,¹ Nicolas Gheeraert,^{1,2,a)}  Sumeru Hazra,¹ Tanay Roy,^{1,b)} Kishor V. Salunkhe,¹ Meghan P. Patankar,¹ and R. Vijay^{1,c)}

AFFILIATIONS

¹Department of Condensed Matter Physics and Materials Science, Tata Institute of Fundamental Research, Homi Bhabha Road, Mumbai 400005, India

²Institut Néel, CNRS and Université Grenoble-Alpes, F-38042 Grenoble, France

^{a)}Present address: Research Center for Advanced Science and Technology (RCAST), The University of Tokyo, Meguro-ku, Tokyo 153-8904, Japan.

^{b)}Present address: Department of Physics and James Franck Institute, University of Chicago, Chicago, Illinois 60637, USA.

^{c)}Author to whom correspondence should be addressed: r.vijay@tifr.res.in.

ABSTRACT

We propose and demonstrate a frequency-multiplexed readout scheme in 3D circuit-quantum electrodynamics (cQED) architecture. We use four transmon qubits coupled to individual rectangular cavities which are aperture-coupled to a common rectangular waveguide feedline. A coaxial to waveguide transformer at the other end of the feedline allows one to launch and collect the multiplexed signal. The reflected readout signal is amplified by an impedance-engineered broadband parametric amplifier with 380 MHz bandwidth. This provides us high fidelity single-shot readout of multiple qubits using compact microwave circuitry, an efficient way for scaling up to more qubits in 3D cQED.

Published under license by AIP Publishing. <https://doi.org/10.1063/1.5089729>

High fidelity quantum measurements are a crucial part of a scalable quantum computing architecture.¹ Apart from determining the state of a quantum register, they are also important for accurate state initialization and quantum error correction. In superconducting circuit technology, the combination of circuit-quantum electrodynamics (cQED)^{2,3} with ultralow noise Josephson Parametric Amplifiers^{4,5} ushered in the era of fast, high fidelity measurements.⁶ This led to the observation of quantum jumps⁷ and quantum feedback,⁸ and enabled accurate state initialization⁹ and error detection.^{10–12} Combined with the nearly six orders of magnitude improvement in coherence times,⁶ superconducting circuits have emerged as one of the leading candidates for building scalable quantum computers. While several proof-of-principle demonstrations of algorithms exist, a practical quantum advantage has not yet been demonstrated due to the small number of qubits used in quantum processors. Multiqubit quantum processors face challenges like variability in device parameters across a chip, efficient use of cryogenic microwave resources, and reduction in gate fidelity due to unwanted crosstalk. A considerable fraction of recent research efforts are focused on solving these scalability related hurdles.

An important step in developing a scalable quantum processor is the implementation of resource-efficient measurement of large number of qubits with high-fidelity. Typical setups require two cryogenic lines to control (input) and measure (output) a single qubit. Furthermore, a third cryogenic line is often needed to bias the first stage parametric amplifier in the output chain. Clearly, this is not a practical solution beyond a few qubits. One solution is to use frequency multiplexing for the measurement lines since the typical bandwidth of readout cavities is about 5–10 MHz. This idea has been previously used in 2D cQED architectures, where several readout resonators coupled to a common feedline are probed using multifrequency pulses.^{13–17} This approach allows one to perform selective readout of any subset of qubits by choosing corresponding frequency components in the readout pulse. Moreover, the multiple frequency components can be generated using one microwave generator modulated by a high bandwidth arbitrary waveform generator which further helps in minimizing resources per qubit. Some architectures have also included Purcell protection¹⁸ by incorporating appropriate filters in the common feed-line¹⁶ or by putting individual Purcell filters for each readout

cavity.¹⁷ While experiments with up to four qubits have been performed in 3D cQED architectures,^{19,20} they have not exploited frequency multiplexing for measurement so far. Furthermore, the modular nature of the 3D cQED architecture can help in solving several scalability related issues to construct a high quality small-scale processor in the near term.

In this letter, we demonstrate a multiplexed readout scheme for transmon qubits²¹ in 3D cQED architecture²² using a rectangular waveguide feed-line as both the multiplexing element²³ and a Purcell filter.²⁴ Four rectangular readout cavities are aperture-coupled to a single rectangular waveguide as shown in Fig. 1. The cavities are composed of two halves, so that the qubits can be placed at the antinode of the field. A coaxial to waveguide transformer at the other end of the waveguide helps address the four separate cavities from a single line. We measured the cavities in reflection and used an impedance-engineered broadband Josephson Parametric Amplifier (JPA)²⁵ to achieve simultaneous single-shot fidelities greater than 98%.

The cavity frequencies are chosen with a spacing of 70–100 MHz to fit within the band of the JPA as shown in Fig. 2. The linewidths ($\kappa/2\pi$) of the readout cavities are adjusted by changing the aperture hole sizes. We first use finite element electromagnetic simulations in COMSOL[®] to set the coupling aperture sizes. The final adjustment is done by tuning the aperture size between each cavity and the waveguide using aluminum tape to get linewidths in the range 5–10 MHz. To obtain a clean response, it is also important to optimize the coaxial to waveguide transition by fine-tuning the length of the coaxial center conductor inserted inside the waveguide.

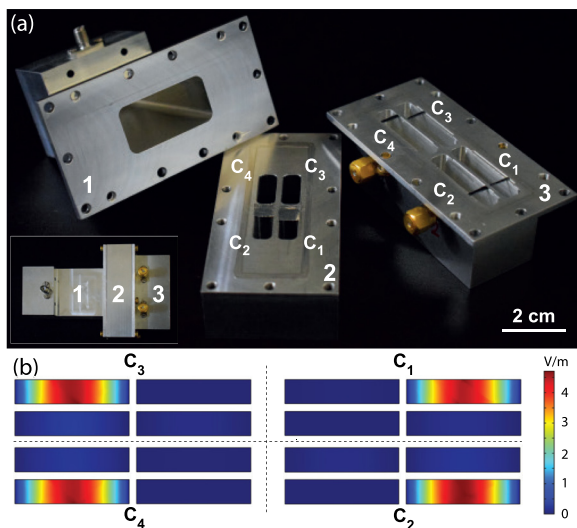


FIG. 1. (a) The four-cavity structure fabricated using aluminum in three separate pieces. Design details can be found in Sec. I of the [supplementary material](#). The piece marked 1 is the rectangular waveguide part with a coaxial port at one end. Piece 2 comprises one half of the readout cavities (C_{1-4}) along with the coupling apertures. Piece 3 comprises the second half of the readout cavities (C_{1-4}) with weakly coupled ports for separate qubit excitation if needed (not used here). The qubits (on silicon chips shown in black color) were positioned to achieve a similar dispersive shift for each cavity. Inset: The fully assembled structure with each interface sealed with indium. (b) Profile of the electric field amplitude at the center of the readout cavities when 10^{-9} Watt excitation is given at the waveguide port. The EM simulation is carried out in COMSOL[®] at each cavity's resonant frequency.

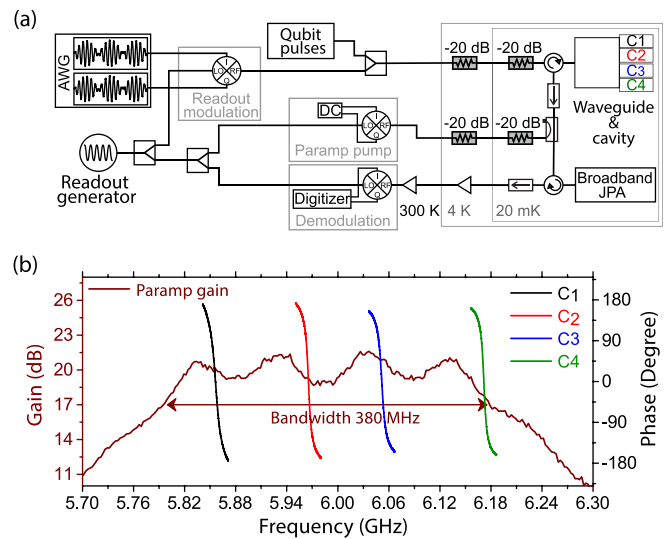


FIG. 2. (a) Setup: Readout tones are generated by sideband modulation technique from one generator which is used for the paramamp pump as well. The reflected signal is amplified, demodulated, and then digitized. (b) Measured gain profile as a function of signal frequency is shown. 20 dB gain and 380 MHz bandwidth are achieved at a pump frequency of 5.984 GHz. Reflected phase responses of four readout cavities (C_{1-4}) as measured from the waveguide port are plotted with respect to the right axis.

To readout multiple qubits simultaneously, we generate a multi-frequency probe pulse (addressing all four cavities) using sideband modulation technique from a central microwave tone. This same central tone is also used as a pump to bias the parametric amplifier [see Fig. 2(a)]. The reflected output signal from the waveguide port is amplified by a broadband Josephson parametric amplifier with an average gain of 20 dB in the relevant bandwidth of 380 MHz around 5.985 GHz and near quantum-limited noise. After several stages of amplification, the output readout signal is down-converted with respect to the central tone, and then digitized after filtering out unwanted frequency components. All cavity signals are finally demodulated in software to recover the amplitude and phase response of each individual cavity. For qubit excitations, we used the same input line as for readout tone, but one can also use separate weakly coupled ports to each individual readout cavity.

At 30 mK temperature, all readout cavities were over-coupled and their frequencies were well-separated from each other with a loaded linewidth ($\kappa/2\pi$) in the intended range of 5–8 MHz. We first characterized each qubit-cavity system separately. The relevant device parameters were then experimentally determined, and are listed in Table I. The values are typical for 3D transmons in cQED architecture. Dispersive shifts ($\chi_{\text{calculated}}$) were calculated using qubit-cavity coupling (g), detuning (Δ) and anharmonicity (α) obtained from the experiment (Table II). The qubit-cavity coupling was extracted from the difference in bare and dressed cavity frequencies. These were followed by time domain measurements on all qubits to determine the coherence properties (Table I). We then used the multiplexing technique to carry out simultaneous measurements of Rabi oscillations on all four qubits, and the data are shown in Fig. 3. Dispersive shifts (χ_{measured}) for all four qubits were also determined using Ramsey

TABLE I. Measured device parameters and coherence numbers of four qubits (Q_1 , Q_2 , Q_3 , and Q_4) in their corresponding readout cavities (C_1 , C_2 , C_3 , and C_4 , respectively). Coherence numbers marked with the superscript “a” were measured one day after the device reached 30 mK, while those marked with the superscript “b” were measured after 15 days. We typically observe such improvements in Ramsey decay time when using aluminum cavities which we believe is due to slow thermalization. The Ramsey decay constants marked with a * showed beating, and were fit using a sinusoidally modulated decaying sine function.

Qubit	Cavity frequency $\omega_c/2\pi$ (GHz)	Cavity linewidth $\kappa/2\pi$ (MHz)	Qubit frequency $\omega_q/2\pi$ (GHz)	Anharmonicity $\alpha/2\pi$ (MHz)	Qubit-cavity coupling $g/2\pi$ (MHz)	T_1^a (μ s)	T_{Ramsey}^a (μ s)	T_{Echo}^a (μ s)	T_{Ramsey}^b (μ s)
Q_1	5.856	8.4	3.752	−318	126	50.1	2.1	3.1	5.7*
Q_2	5.966	5.2	4.122	−306	112	44.1	1.4	2.7	7.6*
Q_3	6.052	7.1	4.880	−292	91	18.8	2.7	3.0	14.4
Q_4	6.172	5.4	5.278	−297	81	25.6	2.6	2.6	12.7

TABLE II. Comparison of calculated and measured dispersive shifts. Dispersive shift for Q_1 could not be extracted cleanly due to beating in the Ramsey fringe. Simultaneously measured readout fidelities are tabulated with their corresponding measurement time and power along with individual measurement fidelities of the four qubits.

Qubit	Dispersive shift $\chi_{\text{calculated}}/2\pi$ (MHz)	Dispersive shift $\chi_{\text{measured}}/2\pi$ (MHz)	Measurement time (ns)	Measurement power (dB m)	Individual readout fidelity (%)	Simultaneous fidelity (%)
Q_1	0.99	...	500	−133.3	98.36	98.05
Q_2	0.98	1.19	350	−137.3	98.72	98.57
Q_3	1.42	1.56	400	−132.8	98.39	98.07
Q_4	1.82	1.76	500	−136.7	98.74	98.68

fringe experiments in the presence of different numbers of cavity photons⁸ and found to be in reasonable agreement with the calculated values ($\chi_{\text{calculated}}$).

We then carried out single-shot measurements to determine readout fidelity for all four qubits. Each experimental sequence starts with a measurement pulse to herald the qubit in the ground state⁹ while the data points which collapse the qubit to the excited state are discarded ($\sim 3\%$ – 5%). With the qubit prepared in the ground

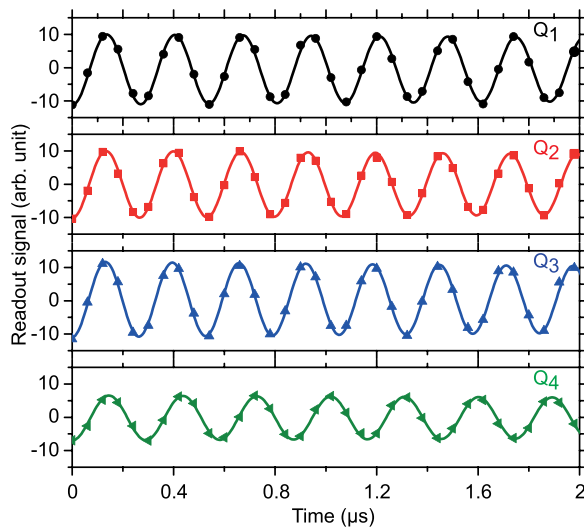


FIG. 3. Simultaneous Rabi oscillations of Q_{1-4} as a function of the corresponding control pulse duration. The signal amplitude of Q_4 is smaller due to a smaller dispersive shift and a reduced JPA gain at 6.172 GHz.

(no pulse on the qubit) or excited state (π pulse on the qubit), we excite the cavity with the readout tone and integrate the reflected signal. This is repeated 3×10^5 times to form histograms of the cavity response for the ground and excited states, respectively. We optimize the measurement time, power, and phase of the readout tone, such that the overlap between the ground and excited state histograms is minimal to ensure maximum readout fidelity. Simultaneously measured histograms for the ground and excited states for all four qubits gave high measurement fidelities ($\sim 98.5\%$), and are shown in Figs. 4(a)–4(d). As shown in Table II, these fidelities are comparable to those obtained from measuring each qubit-cavity system separately without multiplexing.

High fidelity single-shot measurements were further confirmed by observing quantum jumps in simultaneously taken readout traces. After preparing all qubits in their excited states, we turn on the measurement pulses for four cavities simultaneously and acquire the cavity response. As shown in Fig. 4(e), the traces corresponding to four qubits show clear jumps from excited to ground state with no evidence of crosstalk.

We studied crosstalk effects on one qubit arising from both qubit and readout drives applied on other qubits. This was done by performing a Ramsey fringe experiment in the presence of the crosstalk drive. The crosstalk due to other qubit drives was negligible and could be further suppressed by using the weakly coupled ports in each cavity. The crosstalk due to readout drives is shown in Table S1 in the supplementary material. We found significant crosstalk only between cavities C_3 and C_4 and that should be fixable by minor modifications to the positioning of the apertures and optimizing the coaxial to waveguide transition (see Sec. II, supplementary material).

In conclusion, we have demonstrated a frequency-multiplexed readout scheme in 3D cQED architecture using an impedance-engineered broadband parametric amplifier. We simultaneously measured four transmon qubits in four individual cavities coupled to a

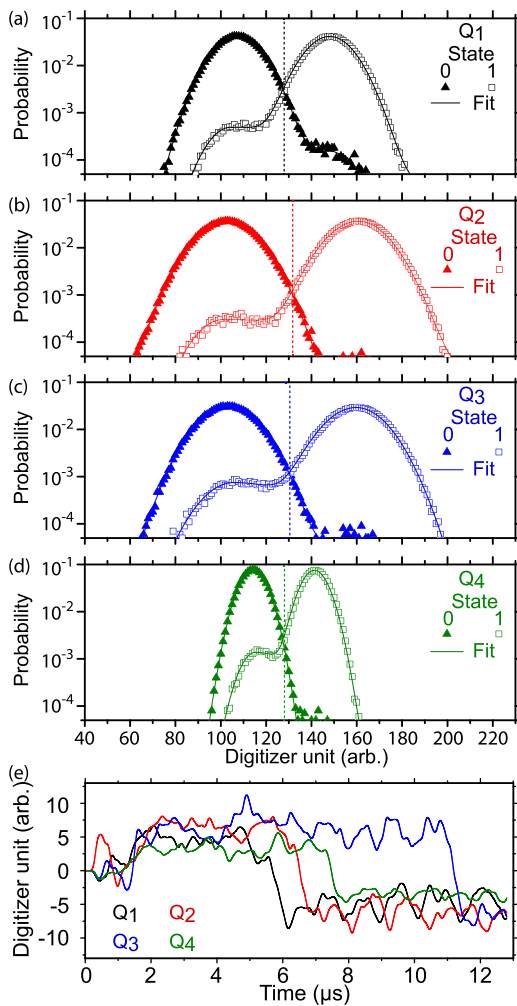


FIG. 4. Measurement histograms: (a)–(d) show the histograms of the integrated single-shot readout signal of Q_1 – Q_4 , respectively, prepared with a π -pulse (empty square) and without (solid triangle), as obtained from 3×10^5 measurements. The histograms are fit to a weighted sum of two Gaussians. The vertical dashed lines indicate the threshold used to discriminate states 0 and 1, and were determined by maximizing the total readout fidelity. (e) Quantum jump: After the qubits are initialized to their excited states, continuous strong measurement tones are applied, and the reflected readout signal is digitized. Abrupt quantum jumps from the excited state to the ground state are clearly visible with no evidence of measurement crosstalk.

single rectangular waveguide. A common input line for qubit and cavity excitations, and more importantly, a single amplifier chain are efficiently used without sacrificing the measurement bandwidth or qubit coherence with negligible crosstalk. A further increase in the number of qubits per measurement line would require careful optimization of the cavity design and improvement of the JPA dynamic range.

See [supplementary material](#) for details of the cavity design and the readout crosstalk data.

This work was supported by the Department of Atomic Energy of the Government of India. R.V. acknowledges support from the Department of Science and Technology, India, via the Ramanujan Fellowship and Nano Mission. N.G. acknowledges support from the Foundation Nanosciences de Grenoble and the Raman Charpak Fellowship. We acknowledge the TIFR nanofabrication facility.

REFERENCES

- ¹M. A. Nielsen and I. L. Chuang, *Quantum Computation and Quantum Information* (Cambridge University Press, 2010).
- ²A. Blais, R.-S. Huang, A. Wallraff, S. M. Girvin, and R. J. Schoelkopf, *Phys. Rev. A* **69**, 062320 (2004).
- ³A. Wallraff, D. I. Schuster, A. Blais, L. Frunzio, R.-S. Huang, J. Majer, S. Kumar, S. M. Girvin, and R. J. Schoelkopf, *Nature* **431**, 162 (2004).
- ⁴M. Hatridge, R. Vijay, D. H. Slichter, J. Clarke, and I. Siddiqi, *Phys. Rev. B* **83**, 134501 (2011).
- ⁵M. A. Castellanos-Beltran and K. W. Lehnert, *Appl. Phys. Lett.* **91**, 083509 (2007).
- ⁶M. H. Devoret and R. J. Schoelkopf, *Science* **339**, 1169 (2013).
- ⁷R. Vijay, D. H. Slichter, and I. Siddiqi, *Phys. Rev. Lett.* **106**, 110502 (2011).
- ⁸R. Vijay, C. Macklin, D. H. Slichter, S. J. Weber, K. W. Murch, R. Naik, A. N. Korotkov, and I. Siddiqi, *Nature* **490**, 77EP (2012).
- ⁹J. E. Johnson, C. Macklin, D. H. Slichter, R. Vijay, E. B. Weingarten, J. Clarke, and I. Siddiqi, *Phys. Rev. Lett.* **109**, 050506 (2012).
- ¹⁰A. Córcoles, E. Magesan, S. J. Srinivasan, A. W. Cross, M. Steffen, J. M. Gambetta, and J. M. Chow, *Nat. Commun.* **6**, 6979 (2015).
- ¹¹D. Ristè, S. Poletto, M.-Z. Huang, A. Bruno, V. Vesterinen, O.-P. Saira, and L. DiCarlo, *Nat. Commun.* **6**, 6983 (2015).
- ¹²J. Kelly, R. Barends, A. Fowler, A. Megrant, E. Jeffrey, T. White, D. Sank, J. Mutus, B. Campbell, Y. Chen *et al.*, *Nature* **519**, 66 (2015).
- ¹³M. Jerger, S. Poletto, P. Macha, U. Hbner, E. Ilichev, and A. V. Ustinov, *Appl. Phys. Lett.* **101**, 042604 (2012).
- ¹⁴Y. Chen, D. Sank, P. O'Malley, T. White, R. Barends, B. Chiaro, J. Kelly, E. Lucero, M. Mariantoni, A. Megrant, C. Neill, A. Vainsencher, J. Wenner, Y. Yin, A. N. Cleland, and J. M. Martinis, *Appl. Phys. Lett.* **101**, 182601 (2012).
- ¹⁵V. Schmitt, X. Zhou, K. Juliusson, B. Royer, A. Blais, P. Bertet, D. Vion, and D. Esteve, *Phys. Rev. A* **90**, 062333 (2014).
- ¹⁶E. Jeffrey, D. Sank, J. Y. Mutus, T. C. White, J. Kelly, R. Barends, Y. Chen, Z. Chen, B. Chiaro, A. Dunsworth, A. Megrant, P. J. J. O'Malley, C. Neill, P. Roushan, A. Vainsencher, J. Wenner, A. N. Cleland, and J. M. Martinis, *Phys. Rev. Lett.* **112**, 190504 (2014).
- ¹⁷J. Heino, C. K. Andersen, A. Remm, S. Krinner, T. Walter, Y. Salathé, S. Gasparinetti, J.-C. Besse, A. Potočnik, A. Wallraff, and C. Eichler, *Phys. Rev. Appl.* **10**, 034040 (2018).
- ¹⁸M. D. Reed, B. R. Johnson, A. A. Houck, L. DiCarlo, J. M. Chow, D. I. Schuster, L. Frunzio, and R. J. Schoelkopf, *Appl. Phys. Lett.* **96**, 203110 (2010).
- ¹⁹H. Paik, A. Mezzacapo, M. Sandberg, D. T. McClure, M. Abdo, A. D. Córcoles, O. Dial, D. F. Bogorin, B. L. T. Plourde, M. Steffen, A. W. Cross, J. M. Gambetta, and J. M. Chow, *Phys. Rev. Lett.* **117**, 250502 (2016).
- ²⁰J. Z. Blumoff, K. Chou, C. Shen, M. Reagor, C. Axline, R. T. Brierley, M. P. Silveri, C. Wang, B. Vlastakis, S. E. Nigg, L. Frunzio, M. H. Devoret, L. Jiang, S. M. Girvin, and R. J. Schoelkopf, *Phys. Rev. X* **6**, 031041 (2016).
- ²¹J. Koch, T. M. Yu, J. Gambetta, A. A. Houck, D. I. Schuster, J. Majer, A. Blais, M. H. Devoret, S. M. Girvin, and R. J. Schoelkopf, *Phys. Rev. A* **76**, 042319 (2007).
- ²²H. Paik, D. I. Schuster, L. S. Bishop, G. Kirchmair, G. Catelani, A. P. Sears, B. R. Johnson, M. J. Reagor, L. Frunzio, L. I. Glazman, S. M. Girvin, M. H. Devoret, and R. J. Schoelkopf, *Phys. Rev. Lett.* **107**, 240501 (2011).
- ²³A. Kou, W. C. Smith, U. Vool, I. M. Pop, K. M. Sliwa, M. Hatridge, L. Frunzio, and M. H. Devoret, *Phys. Rev. Appl.* **9**, 064022 (2018).
- ²⁴A. Narla, S. Shankar, M. Hatridge, Z. Leghtas, K. M. Sliwa, E. Zaly-Geller, S. O. Mundhada, W. Pfaff, L. Frunzio, R. J. Schoelkopf, and M. H. Devoret, *Phys. Rev. X* **6**, 031036 (2016).
- ²⁵T. Roy, S. Kundu, M. Chand, A. M. Vadiraj, A. Ranadive, N. Nehra, M. P. Patankar, J. Aumentado, A. A. Clerk, and R. Vijay, *Appl. Phys. Lett.* **107**, 262601 (2015).